Mutating a Critical Lysine in ShK Toxin Alters Its Binding Configuration in the Pore−Vestibule Region of the Voltage-Gated Potassium Channel, Kv1.3†

Mark D. Lanigan,[‡,§] Katalin Kalman,[||] Yann Lefievre,[⊥] Michael W. Pennington,[⊥] K. George Chandy,[||] and Raymond S. Norton*[,‡,#]

Biomolecular Research Institute, Parkville 3052, Victoria, Australia, Department of Physiology and Biophysics, University of California, Irvine, California 92697, and Bachem Bioscience Inc., King of Prussia, Pennsylvania 19406

Received July 3, 2002; Revised Manuscript Received August 8, 2002

ABSTRACT: The voltage-gated potassium channel in T lymphocytes, Kv1.3, an important target for immunosuppressants, is blocked by picomolar concentrations of the polypeptide ShK toxin and its analogue ShK-Dap22. ShK-Dap22 shows increased selectivity for Kv1.3, and our goal was to determine the molecular basis for this selectivity by probing the interactions of ShK and ShK-Dap22 with the pore and vestibule of Kv1.3. The free energies of interactions between toxin and channel residues were measured using mutant cycle analyses. These data, interpreted as approximate distance restraints, guided molecular dynamics simulations in which the toxins were docked with a model of Kv1.3 based on the crystal structure of the bacterial K^+-channel KcsA. Despite the similar tertiary structures of the two ligands, the mutant cycle data imply that they make different contacts with Kv1.3, and they can be docked with the channel in configurations that are consistent with the mutant cycle data for each toxin but quite distinct from one another. ShK binds to Kv1.3 with Lys22 occupying the negatively charged pore of the channel, whereas the equivalent residue in ShK-Dap22 interacts with residues further out in the vestibule, producing a significant change in toxin orientation. The increased selectivity of ShK-Dap22 is achieved by strong interactions of Dap22 with His404 and Asp386 on Kv1.3, with only weak interactions between the channel pore and the toxin. Potent and specific blockade of Kv1.3 apparently occurs without insertion of a positively charged residue into the channel pore. Moreover, the finding that a single residue substitution alters the binding configuration emphasizes the need to obtain consistent data from multiple mutant cycle experiments in attempts to define protein interaction surfaces using these data.

Suppression of T lymphocyte activity is necessary after organ and tissue transplantation and in the treatment of autoimmune diseases. Regulation of the membrane potential in human T lymphocytes is dominated by homotetramers of the voltage-gated potassium channel, Kv1.3 (*1*, *2*), and blocking this channel can depolarize the T-cell membrane and disrupt the calcium signaling pathway vital for lymphocyte activation (*1*−*5*). Kv1.3 is therefore an important target for immunosuppressive drug design for the treatment of chronic autoimmune diseases such as multiple sclerosis (*6*) and for transplantation therapy (*2*, *7*).

Polypeptide toxins from scorpions, snakes, spiders, cone shells, and sea anemones can potently inhibit voltage-gated potassium channels. These toxins are small (30−60 residues), compact molecules containing 3−4 disulfide bonds but possessing a variety of different protein folds (*8*). All are thought to block K^+ conduction by binding to a loop between the S5 and S6 transmembrane helices, known as the P (pore) region (*1*, *2*). ShK[1] toxin, a 35-residue polypeptide toxin from the sea anemone *Stichodactyla helianthus* (*9*), blocks Kv1.3 at low picomolar concentrations (*10*). The structures of ShK (*11*) and its homologue, BgK (*12*), contain a central helix−kink−helix fold, quite distinct from those of other K^+-channel blocking toxins.

Alanine scanning and other mutagenesis studies have defined the channel-binding surfaces of ShK (*13*−*15*) and BgK (*12*, *16*). They reveal a conserved diad of residues that is essential for K^+-channel blockade. This motif, which is also found in structurally unrelated scorpion toxins such as ChTX, consists of a lysine and a neighboring aromatic residue separated by ∼7 Å (*12*). Recently, Gasparini et al. (*8*) proposed that this motif be more broadly defined as a lysine and a neighboring hydrophobic residue. In the scorpion toxins, Lys27 interacts with a key tyrosine (Tyr400 in Kv1.3) in the K^+-channel ion-selectivity filter (*17*−*19*), located in the pore of the channel. Occlusion of the pore by the lysine residue is presumably the mechanism by which K^+ efflux is blocked by these toxins. ShK is thought to behave in a similar fashion via the interaction of Lys22 with the Kv1.3 pore (*10*).

† This work was supported in part by National Institutes of Health Grant GM54221 (to W. R. Kem, M.W.P., R.S.N., and K.G.C.).

* To whom correspondence should be addressed.

‡ Biomolecular Research Institute.

§ Present address: Australian Animal Health Laboratory, Geelong 3220, Australia.

|| University of California, Irvine.

⊥ Bachem Bioscience Inc.

Present address: The Walter and Eliza Hall Institute of Medical Research, NMR Laboratory, 381 Royal Parade, Parkville 3052, Australia. Phone: +61-3-9903 9650. FAX: +61-3-9903 9655. Email: Ray.Norton@wehi.edu.au.

[1] Abbreviations: ShK toxin, *Stichodactyla helianthus* K^+ channel toxin; ShK-Dap22, ShK toxin analogue with 1,3-diaminopropionic acid (Dap) at position 22; MD, molecular dynamics.

10.1021/bi026400b CCC: $22.00
Published on Web 09/13/2002

A synthetic analogue of ShK containing a single 1,3-diaminopropionic acid (Dap) substitution in place of the critical Lys22, ShK-Dap22 (*10*), has a global fold similar to that of native toxin, but with some differences in the relative orientations of key binding side chains (*10*). ShK-Dap22 is much more selective than ShK, having only slightly lower potency against Kv1.3 (*10*, *20*) but significantly reduced potency against other ShK-sensitive channels such as Kv1.1, Kv1.4, and Kv1.6. In recent proof-of-concept studies, ShK and ShK-Dap22 were reported to prevent and treat experimental autoimmune encephalomyelitis in rats, a model for the chronic autoimmune disease multiple sclerosis (*6*).

In this paper, we have investigated the binding of both ShK and ShK-Dap22 to Kv1.3 using thermodynamic mutant cycle analyses (*21*) coupled with restrained molecular dynamics and a model of this channel (*10*, *22*). Our goal was a better understanding of the interactions between Kv1.3 and ShK versus ShK-Dap22 in order to guide the design of specific toxin mutants with the potential to be used therapeutically as immunosuppressants. An unexpected outcome, however, was that shortening the side chain at position 22 resulted in the channel pore not being occupied, which allowed the toxin to reorient in the external vestibule of the channel. This result has more general implications for the application of mutant cycle analysis to defining protein−protein interactions.

MATERIALS AND METHODS

Peptide Synthesis. Analogues of ShK and ShK-Dap22 were synthesized, purified, and characterized as reported previously (*10*, *13*, *14*). Samples were weighed and adjusted to account for peptide content prior to bioassay. One-dimensional ^{1}H NMR spectra of several analogues were recorded to confirm their correct folding.

Electrophysiology Data and Cell Culture. Mutations of Kv1.3 were generated by the two-step PCR method (*17*). cRNAs of wild-type and mutant Kv1.3 were transcribed in vitro using mMACHINE Kit (AMBION Inc., Austin, TX) and injected into oocytes (*Xenopus laevis* from Nasco, Fort Atkinson, WI). Oocytes with 5−10 μA were selected for toxin binding measurements. K^+ currents were measured at room temperature using the two-electrode voltage-clamp technique (*10*, *17*), and the data were analyzed by pClamp software (Axon Instruments, Union City, CA). Whole oocytes were held at −100 mV and depolarized to +40 mV over 500 ms, with a pulse interval of 30 s. Capacitative and leak currents were subtracted prior to analysis using the P/4 procedure. ND96 (in mM: 96 NaCl, 2 KCl, 1.8 $CaCl_2$, 1 $MgCl_2$, 5 HEPES, 0.1% w/v bovine serum albumin, pH 7.6) was used as the oocyte bathing solution and as the solvent for toxins. The dissociation constant was calculated assuming a 1:1 binding of toxin to Kv1.3.

Mutant Cycle Analysis. Thermodynamic mutant cycle analyses were performed as described previously (*10*) for mutants of ShK, ShK-Dap22, and Kv1.3. To define the orientation of ShK-Dap22, we tested ShK-Dap22 as wild type and ShK-Dap22-X as mutants (Dap22-R11A, Dap22-R29A, Dap22-S20A, Dap22-F27A) on Kv1.3, and K_d values were calculated. Interactions between Asp386 and several residues of ShK-Dap22 proved to be important in defining the orientation of this toxin in the pore−vestibule region, as described below. Because of this, their validity was checked with two different channel mutants, D386K and D386N, with similar results being obtained for both mutants; both mutations produce slow inactivating channels.

The following Kv1.3 residues were replaced by PCR mutagenesis: Ser379 → Ala379, Asp386 → Lys386, Asp386 → Asn386, Tyr400 → Val400, Asp402 → Asn402, His 404 → Val404. As substitutions at positions 400 and 402 result in nonfunctional channels, dimeric constructs were generated containing one wild-type subunit and one mutant subunit, the resulting tetramers being composed of ($Asn402_2$ − $Asp402_2$) and ($Val400_2$ − $Tyr400_2$). These channel mutants have been described in mapping studies with scorpion toxins (*17*, *19*).

Mutant cycles for Kv1.3-ShK were as follows: Kv1.3 (Ser379 → Ala379) − ShK (Arg11 → Ala11), Kv1.3 (Ser379 → Ala379) − ShK (Arg29 → Ala29), Kv1.3 (Asp386 → Asn386) − ShK (Arg11 → Ala11), Kv1.3 (Asp386 → Asn386) − ShK (Ser20 → Ala20), Kv1.3 (Asp386 → Asn386) − ShK (Phe27 → Ala27), Kv1.3 (Asp386 → Asn386) − ShK (Arg29 → Ala29), Kv1.3 (Asp386 → Lys386) − ShK (Lys9 → Ala9), Kv1.3 (Asp386 → Lys386) − ShK (Arg11 → Ala11), Kv1.3 (Asp386 → Lys386) − ShK (Lys22 → Nle22), Kv1.3 (Asp386 → Lys386) − ShK (Orn22 → Nle22), Kv1.3 (Asp386 → Lys386) − ShK (Arg29 → Ala29), Kv1.3 (Tyr400 → Val400) − ShK (Lys9 → Ala9), Kv1.3 (Tyr400 → Val400) − ShK (Arg11 → Ala11), Kv1.3 (Tyr400 → Val400) − ShK (Lys22 → Nle22), Kv1.3 (Tyr400 → Val400) − ShK (Orn22 → Nle22), Kv1.3 (Asp402 → Asn402) − ShK (Lys9 → Ala9), Kv1.3 (Asp402 → Asn402) − ShK (Arg11 → Ala11), Kv1.3 (Asp402 → Asn402) − ShK (Lys22 → Nle22), Kv1.3 (Asp402 → Asn402) − ShK (Orn22 → Nle22), Kv1.3 (His404 → Val404) − ShK (Lys9 → Ala9), Kv1.3 (His404 → Val404) − ShK (Arg11 → Ala11), Kv1.3 (His404 → Val404) − ShK (Ser20 → Ala20), Kv1.3 (His404 → Val404) − ShK (Lys22 → Nle22), Kv1.3 (His404 → Val404) − ShK (Orn22 → Nle22), Kv1.3 (His404 → Val404) − ShK (Phe27 → Ala27), Kv1.3 (His404 → Val404) − ShK (Arg29 → Ala29).

Mutant cycles for Kv1.3-ShK-Dap22 were as follows: Kv1.3 (Ser379 → Ala379) − ShK-Dap22 (Arg29 → Ala29), Kv1.3 (Asp386 → Asn386) − ShK-Dap22 (Arg11 → Ala11), Kv1.3 (Asp386 → Asn386) − ShK-Dap22 (Ser20 → Ala20), Kv1.3 (Asp386 → Asn386) − ShK-Dap22 (Phe27 → Ala27), Kv1.3 (Asp386 → Asn386) − ShK-Dap22 (Arg29 → Ala29), Kv1.3 (Asp386 → Lys386) − ShK-Dap22 (Arg11 → Ala11), Kv1.3 (Asp386 → Lys386) − ShK-Dap22 (Dap22 → Nle22), Kv1.3 (Asp386 → Lys386) − ShK-Dap22 (Arg29 → Ala29), Kv1.3 (Tyr400 → Val400) − ShK-Dap22 (Dap22 → Nle22), Kv1.3 (Asp402 → Asn402) − ShK-Dap22 (Arg11 → Ala11), Kv1.3 (Asp402 → Asn402) − ShK-Dap22 (Dap22 → Nle22), Kv1.3 (His404 → Val404) − ShK-Dap22 (Arg11 → Ala11), Kv1.3 (His404 → Val404) − ShK-Dap22 (Ser20 → Ala20), Kv1.3 (His404 → Val404) − ShK-Dap22 (Dap22 → Nle22), Kv1.3 (His404 → Val404) − ShK-Dap22 (Phe27 → Ala27), Kv1.3 (His404 → Val404) − ShK-Dap22 (Arg29 → Ala29).

In our oocyte preparations, ShK blocked Kv1.3 currents with a K_d of 11 ± 1.4 pM (n = 4, mean ± SE), and ShK-Dap22 blocked Kv1.3 currents with a K_d of 3.3 ± 1.9 pM (n = 12), in both cases with a 1:1 stoichiometry. This gives an indication of typical errors for replicate experiments, but

the actual K_d value for a given batch of toxin varied from one oocyte preparation to another. In each experiment, therefore, the K_d for wild-type toxin on wild-type channel was measured and used to calculate the change in coupling energy, $\Delta\Delta G$, for a given pair of residues and their mutants, all measured on the same oocyte preparation. These coupling energies were calculated using the formula: $\Delta\Delta G = RT \ln \Omega$, where Ω is a dimensionless value given by the formula $\Omega = [K_d(\text{Wt ShK}-\text{Wt Kv1.3}) \times K_d(\text{mut ShK}-\text{mut Kv1.3})]/[K_d(\text{mut ShK}-\text{Wt Kv1.3}) \times K_d(\text{Wt ShK}-\text{mut Kv1.3})]$, where mut and Wt refer to mutant and wild-type, respectively (*21*). Each $\Delta\Delta G$ value was the mean of at least 3−4 sets of measurements.

Molecular Modeling and Docking Simulations. The closest-to-average conformations of ShK and ShK-Dap22 from the families of NMR-derived structures (*10*, *11*) were docked to our model of Kv1.3 (*22*) using restrained molecular dynamics, essentially as described previously (*10*, *22*). Briefly, ShK was juxtaposed with the Kv1.3 model such that Lys22 was facing the pore and Arg11 was close to both His404 and Asp386. Intermolecular distance constraints were applied in accordance with data from thermodynamic mutant cycle analyses. Schreiber and Fersht (*21*) found a strong correlation between $\Delta\Delta G$ values obtained by mutant cycle analysis and the interresidue distance derived from crystal structures of barnase and barstar, with $\Delta\Delta G$ values of ≥ 0.5 kcal·mol^{-1} corresponding to an interresidue distance of ≤ 5 Å, and higher $\Delta\Delta G$ values matching shorter interresidue distances. To be conservative, a $\Delta\Delta G$ value of ≥ 0.8 kcal·mol^{-1} was used in this work as an indicator of a close interaction between a pair of toxin and channel residues. Note that, although high $\Delta\Delta G$ values indicate tight interactions, residues that are physically close may be energetically "silent" and thus not detected by this method (*18*, *21*).

In this way, upper bound distance constraints of 6.0 Å were applied between the following pairs of toxin and channel atoms: ShK-Kv1.3 Lys22 N^{ζ}−Tyr400 X (from four subunits, where X is the centroid of the aromatic ring); Arg11 C^{ζ} to His404 $N^{\delta 1}$; Arg11 C^{ζ} to Asp386 C^{γ}; Arg11 C^{ζ} to Ser379 O^{γ}; Arg29 C^{ζ} to Asp386 C^{γ}. For ShK-Dap22-Kv1.3: Dap22 N^{γ} to His404 $N^{\delta 1}$, Dap22 N^{γ} to Asp386 C^{γ}, Dap22 N^{γ} to Asp402 C^{γ}, Arg11 C^{ζ} to Asp386 C^{γ}, Arg11 C^{ζ} to His404 $N^{\delta 1}$, Arg29 C^{ζ} to Asp386 C^{γ}, Ser20 O^{γ} to Asp386 C^{γ}, Ser20 O^{γ} to His404 $N^{\delta 1}$, and Phe27 X to Asp386 C^{γ}. The restrained toxin−channel complex was then subjected to 250 ps of in vacuo molecular dynamics in the CVFF forcefield of Discover (MSI) as described previously (*22*). The initial orientation of ShK-Dap22 was the same as for ShK, i.e., with residue 22 facing the pore. In the case of ShK, several different initial orientations were tested, with little influence on the final docking configuration.

Surface areas and solvent accessibilities for each residue of ShK, ShK-Dap22, or Kv1.3 were calculated in MOLMOL 2.6 (*23*) from Connolly surfaces generated with a 1.4 Å probe radius. The shape complementarities of the ShK-Kv1.3 and ShK-Dap22-Kv1.3 binding interfaces were calculated using the program SC (*24*).

RESULTS AND DISCUSSION

ShK−Kv1.3 Interactions. Our initial investigation of the interaction of ShK and ShK-Dap22 with Kv1.3 identified several key toxin−channel interactions, from which a preliminary docking of ShK with a crude model of Kv1.3 was derived (*10*). A newer model of Kv1.3 has since been generated based on the KcsA crystal structure (*22*), and a preliminary docking of ShK in this model suggested additional toxin−channel interactions that could be tested via mutant cycle analyses in order to refine the docked configuration. Figure 1 summarizes all pairwise interactions tested between ShK or ShK-Dap22 and Kv1.3.

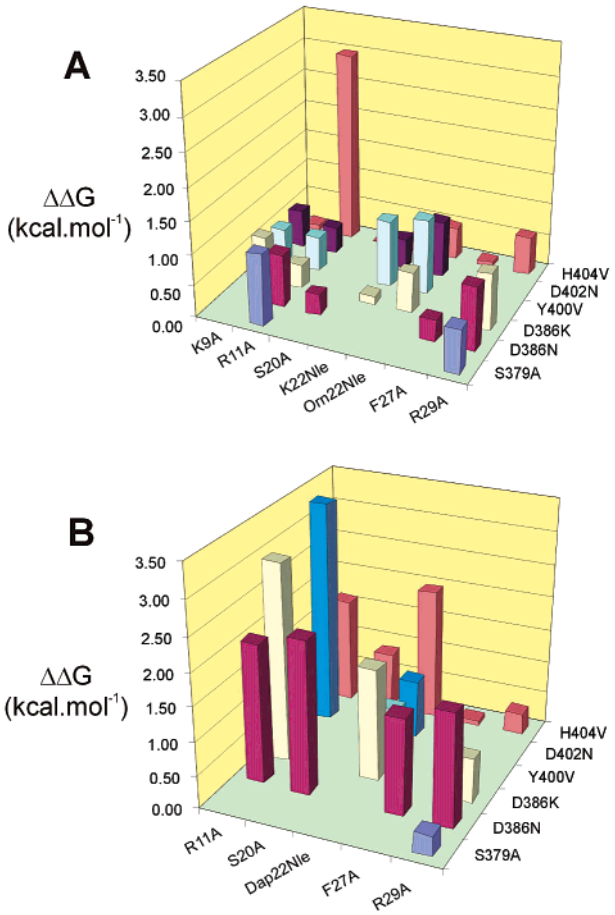

FIGURE 1: Coupling energies $\Delta\Delta G$ (kcal·mol^{-1}) for toxin−channel interactions. (A) ShK and Kv1.3 mutants, and (B) ShK-Dap22 and Kv1.3 mutants. All pairs of interactions probed by mutant cycle analyses are represented by bars in this figure; blank entries represent interactions not tested. The bar for the ShK-Dap22−Tyr400 interaction is partially obscured in (B) but corresponds to a $\Delta\Delta G$ value of 0.76 kcal·mol^{-1}. The bars for a given Kv1.3 mutant are the same color, and identical colors are used in parts A and B except for D402N, which is purple in (A) and dark blue in (B).

Arg11 of ShK couples strongly with His404 in the channel vestibule (Figure 1A). The shortest distance between His404 side chains from adjacent channel subunits is approximately 11 Å, raising the possibility that Arg11 might be coupled to two His404 residues. From the preliminary model of ShK docked to Kv1.3, the coupling of Arg11 to a single His404 brings the former into proximity to both Ser379 and Asp386 of the same subunit (distance from His404 $N^{\delta 1}$ to Ser379 O^{γ} is 3.6 Å and to Asp386 C^{γ}, 9.1 Å). Mutant cycle analyses yielded $\Delta\Delta G$ values for Arg11−Ser379 and Arg11−Asp386 of 1.12 and 0.82 kcal·mol^{-1}, respectively, indicating that these pairs of residues are indeed energetically coupled. The Arg11−Ser379 coupling in particular confirms that Arg11 is coupled to His404 from one subunit and not two.

The coupling of Arg11 with His404 from a single subunit placed Arg29 near Asp386 from an adjacent channel subunit. This Arg29−Asp386 interaction was confirmed by $\Delta\Delta G$ values of 0.89 and 1.00 kcal·mol^{-1} using R29A−D386K and R29A−D386N mutant cycles, respectively. The observed coupling of Arg29 to Asp386 would be expected to bring the former into proximity to both His404 and Ser379; $\Delta\Delta G$ values of 0.59 and 0.68 kcal·mol^{-1} for Arg29−His404 and Arg29−Ser379, respectively, suggest that these residues are coupled, albeit weakly.

The contributions of Ser20 and Phe27, which are also important for channel binding by ShK (*13*−*15*), were investigated with mutant cycles involving these two residues and either Asp386 or His404. As shown in Figure 1A, the low $\Delta\Delta G$ values for the Ser20−Asp386, Ser20−His404, Phe27−Asp386, and Phe27−His404 mutant cycles indicate that neither ShK residue is energetically coupled to Asp386 or His404.

ShK-Dap^{22}−Kv1.3 Interactions. Our previous work (*10*) showed a decrease in the strength of the coupling between Dap22 and Tyr400 compared with that between Lys22 in ShK and Tyr400, suggesting that residue 22 was not oriented into the pore-lumen and therefore was no longer closely interacting with the selectivity-filter residues. Additional mutant cycles were undertaken to further define the binding configuration of ShK-Dap22 (Figure 1B). As with ShK, Arg11 of ShK-Dap22 coupled strongly to both Asp386 and His404 ($\Delta\Delta G$ = 2.08 and 2.98 kcal·mol^{-1} for R11A−D386N and R11A−D386K, respectively, and 1.59 kcal·mol^{-1} for His^{404}), but with quite different relative coupling energies from those in ShK (compare Figures 1A and 1B). Also in contrast to ShK, Arg11 of ShK-Dap22 coupled strongly to Asp402 ($\Delta\Delta G$ = 3.34 kcal·mol^{-1}). Arg29 of ShK-Dap22 coupled to Asp386 ($\Delta\Delta G$ = 1.68 kcal·mol^{-1}), but not Ser379 or His404 ($\Delta\Delta G$ = 0.29 and 0.32 kcal·mol^{-1}, respectively). Both Ser20 and Phe27 coupled strongly to Kv1.3 Asp386 ($\Delta\Delta G$ = 2.27 and 1.45 kcal·mol^{-1}, respectively), and Ser20 coupled weakly to His404 ($\Delta\Delta G$ = 0.87 kcal·mol^{-1}), whereas in ShK neither Ser20 nor Phe27 showed significant couplings. Thus, as illustrated in Figure 1, there were major differences in the pattern of interactions between ShK and ShK-Dap22, suggesting that they might bind to Kv1.3 in different configurations.

Docking of ShK and ShK-Dap22 with Kv1.3. The structure of ShK docked with a model of Kv1.3 (*22*) using the complete set of restraints is shown in Figure 2A. This binding configuration differs from the preliminary version (*10*) in the location of Arg11 with respect to His404. In the preliminary model, Arg11 was close to both His404 and Ser379 but approximately 12 Å from Asp386. The application of a distance constraint between Arg11 and Asp386 reduces that distance while still allowing the toxin residue to be close to His404 and Ser379. Our new docking is also based on an improved Kv1.3 model that more accurately mimics the KcsA structure (*22*).

Superimposing ShK bound to Kv1.3 in the refined model against the toxin's initial structure showed that bound ShK deviated from its starting conformation during docking (2.6 Å RMSD over the backbone). The deviation of the α-helical region of the molecule (residues 14−24) was less (1.2 Å), indicating that structural changes were greater in the toxin's N- and C-termini. To further examine these deviations, ShK

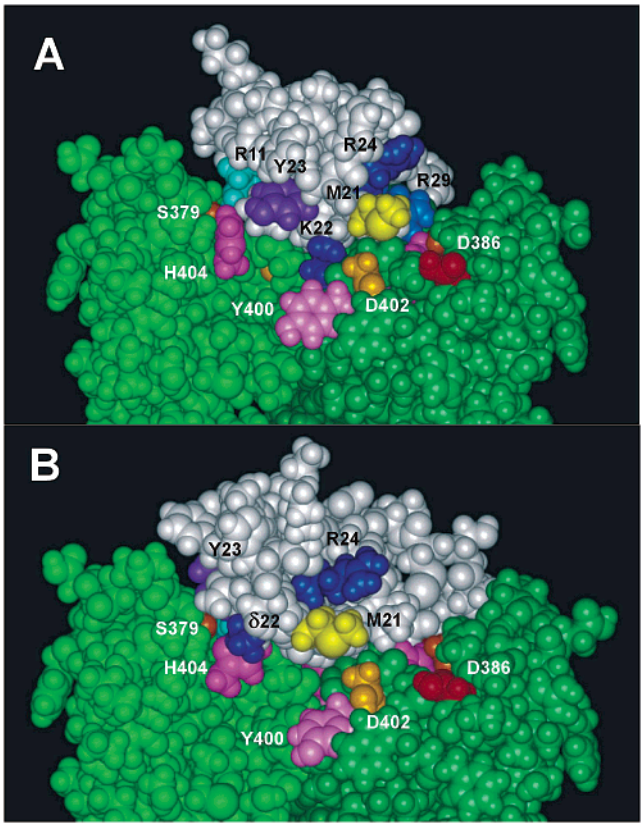

FIGURE 2: Side views of ShK (A) and ShK-Dap22 (B) docked into the Kv1.3 model (*22*). The channel subunit nearest the viewer is removed. Toxin and channel side chains are colored as follows: ShK and ShK-Dap22, Arg11 cyan, Lys22 or Dap22 (δ) and Arg24 blue, Tyr23 purple, Met21 yellow; Kv1.3, Asp386 red, Asp402 gold, His404 magenta, and Ser379 orange. In this view, the side chains of Tyr23 and Arg11 of ShK and ShK-Dap22 are partially obscured. The channel subunits are colored different shades of green.

was subjected to two restrained MD simulations in the absence of Kv1.3, with either 19 or 34 intramolecular distance constraints applied to the toxin, identical to those used in the docking simulations. In the absence of Kv1.3 and intermolecular distance constraints, ShK still deviated from its initial conformation, albeit to a lesser extent (1.4 Å), and the deviations were again smaller for residues 14−24.

ShK-Dap22 was docked with Kv1.3 in the same way as for ShK but using the restraints summarized in Figure 1B. The structure, shown in Figure 2B, satisfied all of the applied distance constraints (maximum final distance 6.3 Å). As with ShK, ShK-Dap22 deviated up to 2.9 Å from its starting conformation during the docking simulation, with the region between residues 14 and 24 again less affected (1.5 Å RMSD over the backbone). In a restrained MD simulation of ShK-Dap22 in the absence of Kv1.3, the structure diverged by a similar extent to that of the native toxin.

The mutant cycle data in Figure 1 strongly imply that ShK and ShK-Dap22 bind to Kv1.3 in different orientations. To establish that these differences were genuine, and that the two sets of constraints could not be satisfied by a common docked configuration, the structure of ShK-Dap22 was superimposed on the conformation of ShK bound to Kv1.3 (Figure 2A). Key intermolecular distances between Kv1.3 and the superimposed ShK-Dap22 were measured and are summarized in Table 1 along with those obtained for the ShK-Dap22−Kv1.3 model (Figure 2B). Orienting ShK-

Table 1: Summary of Intermolecular Distances in the ShK-Dap22-Kv1.3 Model[a] and Equivalent Distances for ShK-Dap22 When Superimposed[b] over ShK in the Refined ShK−Kv1.3 Complex

interaction	ΔΔ*G* (kcal·mol^{-1})[c]	ShK-Dap22 (Å)	ShK-Dap22$_{(ShK)}$[d] (Å)
11 C^{ζ} ··· 379$_A$ O^{γ}		5.1	8.8
11 C^{ζ} ··· 386$_A$ C^{γ}	2.98	6.2	15.4
11 C^{ζ} ··· 402$_A$ C^{γ}	3.38	6.1	15.1
11 C^{ζ} ··· 404$_A$ $N^{\delta1}$	1.59	6.2	8.2
20 O^{γ} ··· 386$_D$ C^{γ}	2.27	6.3	11.6
20 O^{γ} ··· 404$_D$ $N^{\delta1}$	0.87	6.1	12.1
22 N^{γ} ··· 386$_D$ C^{γ}	1.69	6.3	12.2
22 N^{γ} ··· 400$_A$ X		16.6	10.8
22 N^{γ} ··· 400$_B$ X		17.7	11.5
22 N^{γ} ··· 400$_C$ X		11.2	8.6
22 N^{γ} ··· 400$_D$ X		9.3	7.6
22 N^{γ} ··· 402$_D$ C^{γ}	0.87	4.3	5.2
22 N^{γ} ··· 404$_A$ $N^{\delta1}$	1.98	6.1	6.5
27 X ··· 386$_A$ C^{γ}	1.45	6.3	8.5
29 C^{ζ} ··· 386$_B$ C^{γ}	1.68	6.1	12.4

[a] Channel subunits (A−D) are indicated in subscript. [b] Over the backbone heavy atoms of residues 3−33. [c] Values taken from Figure 1. [d] Distances between ShK-Dap22 and Kv1.3 for ShK-Dap22 superimposed over ShK in the ShK−Kv1.3 model (Figure 2A).

Table 2: Summary of Intermolecular Distances in the ShK−Kv1.3 Model[a] and Equivalent Distances for ShK When Superimposed over ShK-Dap22[b] in the ShK-Dap22−Kv1.3 Model

interaction	ΔΔ*G* (kcal·mol^{-1})[c]	ShK (Å)	ShK$_{(ShK-Dap22)}$[d] (Å)
11 C^{ζ} ··· 379$_A$ O^{γ}	1.12	5.4	9.8
11 C^{ζ} ··· 386$_A$ C^{γ}	0.82	6.2	16.5
11 C^{ζ} ··· 402$_A$ C^{γ}		7.1	15.0
11 C^{ζ} ··· 404$_A$ $N^{\delta1}$	2.98	6.2	8.3
20 O^{γ} ··· 386$_D$ C^{γ}		12.6	12.6
20 O^{γ} ··· 404$_D$ $N^{\delta1}$		11.6	6.7
22 C^{γ} ··· 386$_D$ C^{γ}		15.4	14.6
22 C^{γ} ··· 400$_A$ X		8.3	11.7
22 C^{γ} ··· 400$_B$ X		7.8	12.5
22 C^{γ} ··· 400$_C$ X		8.1	12.0
22 C^{γ} ··· 400$_D$ X		8.6	11.1
22 C^{γ} ··· 402$_D$ C^{γ}		8.1	8.9
22 C^{γ} ··· 404$_A$ $N^{\delta1}$		9.9	8.4
27 X ··· 386$_A$ C^{γ}		10.8	13.3
29 C^{ζ} ··· 386$_B$ C^{γ}	1.00	6.0	10.8
22 N^{ζ} ··· 400$_{A,B,C,D}$ X	1.04	6.5 ± 0.1	

[a] Channel subunits (A−D) are indicated in subscript. [b] Over the backbone heavy atoms of residues 3−33. [c] Values taken from Figure 1. [d] Distances between ShK and Kv1.3 for ShK superimposed over ShK-Dap22 in the ShK-Dap22−Kv1.3 model (Figure 2B).

Dap22 with Kv1.3 so as to mimic the ShK binding configuration resulted in most of the ShK-Dap22 constraints being violated by between 2 and 9 Å (Table 1), while in the ShK-Dap22 binding configuration (Figure 2B) they were satisfied. Thus, the experimentally derived restraints which define the ShK-Dap22 interaction were not satisfied upon superposition with the ShK−Kv1.3 model.

The converse is also true. When ShK was superimposed on the conformation of ShK-Dap22 bound to Kv1.3 (Figure 2B), distances between Arg11 of ShK and vestibule residues Ser379, Asp386, and His404 were violated by up to 10 Å (Table 2). Similarly, C^{γ} of Lys22 (equivalent to N^{γ} of Dap^{22}) is 3−5 Å further away from Tyr400 with ShK in the ShK-Dap22 orientation. The docked orientation of ShK-Dap22 with Kv1.3 would not allow observed ShK−Kv1.3 interactions to be satisfied.

Comparison of ShK and ShK-Dap22 Channel-Binding Configurations. Both polypeptides bind in the same general region of Kv1.3, interacting predominantly with two adjacent subunits of the channel. While both molecules physically block the opening of the channel-pore, the region of ShK-Dap22 containing the Dap residue is oriented further from the pore than ShK and more toward the vestibule, under the influence of interactions between Dap22 and both His404 and Asp386 (Figure 3). As a result, there is a slight tipping of ShK-Dap22 relative to the native toxin and a rotation of about 20° normal to the pore axis (Figure 3A). As Lys22 of ShK occupies the pore lumen (as reflected by coupling with Tyr400), this region of the toxin is oriented over the center of the channel. Despite the fact that Dap22 does not occupy the pore, ShK-Dap22 still occludes the entrance to the pore (Figure 3). In fact, there is no side chain in ShK-Dap22 that appears to be capable of occupying the mouth of the pore in the way that Lys22 of ShK does. ShK-Dap22 is therefore able to effect potent and selective blockade of Kv1.3 without occupying the pore lumen.

Ligand- and Channel-Binding Surfaces. The differences between the solvent-accessible surface areas of ShK and Kv1.3 in the free and docked structures are 860 and 740 Å^2, respectively, and the corresponding values for ShK-Dap22 are 860 and 750 Å^2. Thus, despite the apparent differences in the binding configurations (Figures 2, 3), approximately equal surface areas of each ligand are buried upon binding. Moreover, these values are consistent with literature values for other protein−protein interactions (*25*, *26*). Changes in the solvent-accessible surface area of ShK-bound Kv1.3 are found mostly on a single-channel subunit, namely, that containing the Arg29−Asp386 coupling (Figure 3C). Interestingly, despite the fact that most of the ShK-vestibule constraints are to the adjacent subunit (by virtue of Arg11 interactions with Ser379, Asp386, and His404), residues in this subunit experience little change in their solvent accessibility (Figure 3C). By comparison, the changes in solvent-accessible surface area for ShK-Dap22-bound Kv1.3 are more evenly distributed over the four subunits of the channel vestibule. Despite the different bound configurations of ShK and ShK-Dap22 to Kv1.3, the binding surfaces of the ligands are similar; of the total number of residues involved in the channel-binding surfaces of the 2 models (13 for ShK, 17 for ShK-Dap22), 10 are shared between them, namely, Arg1, Arg11, Met21, Lys/Dap22, Tyr23, Leu25, Ser26, Phe27, Arg29, and Lys30.

To determine the shape complementarity of ShK and ShK-Dap22 bound to Kv1.3, the parameter S_c (*24*) was determined. $S_c = 1$ for surfaces that are precisely matched and 0 for surfaces with essentially no topographical correlation. S_c was 0.69 for the ShK−Kv1.3 interface and 0.62 for ShK-Dap22. The value for the ShK−Kv1.3 model is just outside the range observed by Lawrence and Colman (*24*) for good complementarity in protein/protein-inhibitor complexes. For instance, bovine pancreatic β-trypsin and trypsin inhibitor were found to have good complementarity with $S_c = 0.76$, as were α-chymotrypsin and ovomucoid with $S_c = 0.71$. The value of $S_c = 0.62$ for the ShK-Dap22 model is more representative of that observed for antigen−antibody complexes (*27*) and suggests lower shape complementarity between toxin and channel in this binding configuration. The weak shape complementarity observed in these models

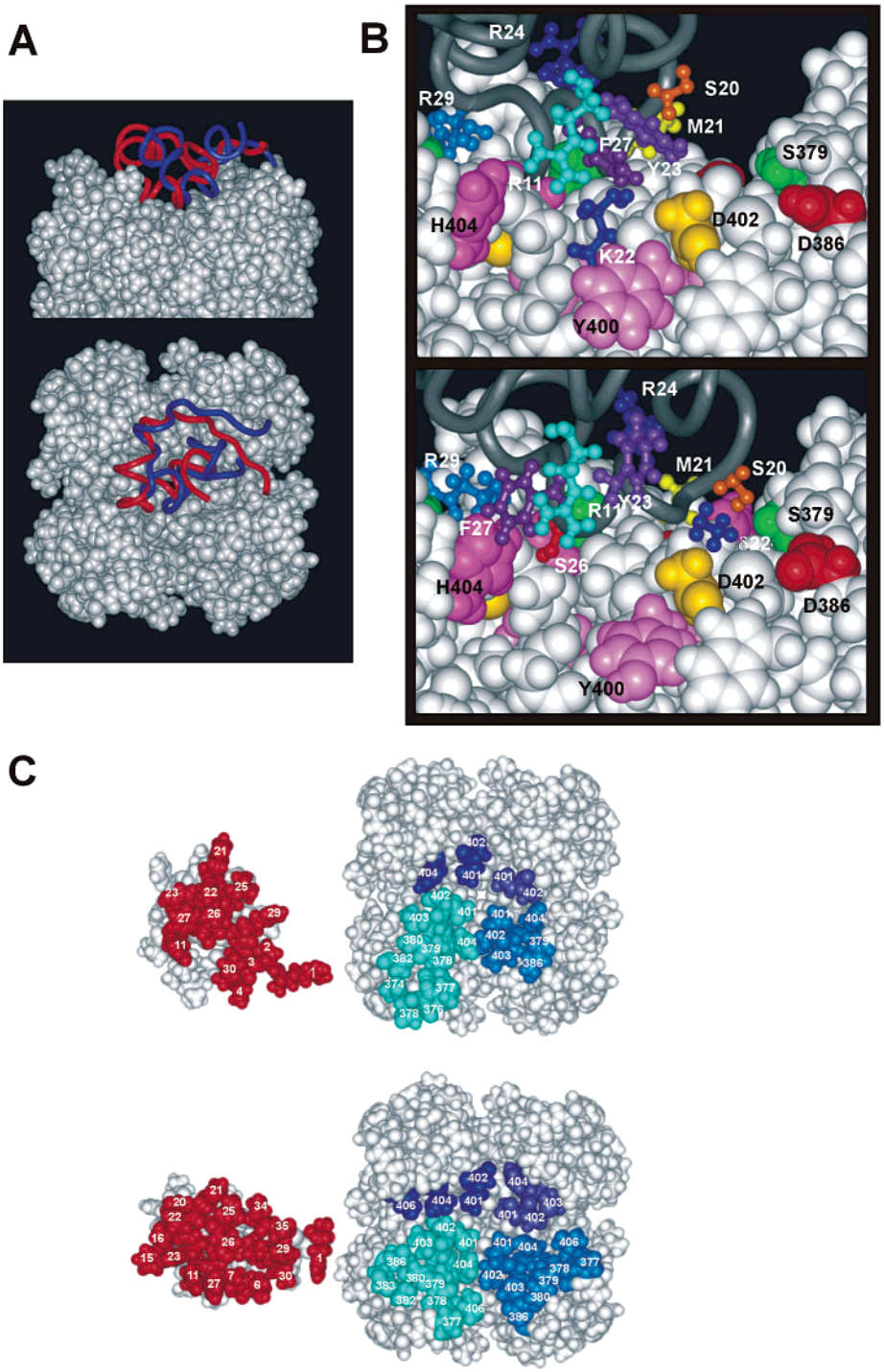

FIGURE 3: Comparison of the bound configurations of ShK and ShK-Dap22 with Kv1.3. (A) The channel (white) is viewed from the side (top panel) and above (bottom panel) in CPK representation. The bound configurations of ShK (blue) and ShK-Dap22 (red) are shown as backbone ribbons; the two ligand molecules are superimposed over the backbone heavy atoms of residues 3−33. (B) Close-up of the interactions between ShK (top) and ShK-Dap22 (bottom) with a model of the S5−P−S6 regions of Kv1.3. The channel (white) is viewed from the side in space-filling representation with the subunit nearest the reader removed for clarity. Channel side chains are colored as follows: Ser379 green, Asp386 red, Tyr400 pink, Asp402 gold, and His404 magenta. Selected toxin side chains are shown in ball-and-stick configuration and are colored as follows: Arg11 cyan, Ser20 orange, Met21 yellow, Dap (δ)/Lys22 blue, Tyr23 and Phe27 purple, Arg24 dark blue, Ser26 red (ShK-Dap22 only), and Arg29 light blue. Note that Lys22 in the top panel indicates the location of the pore and that the channel orientations are the same in the top and bottom panels. (C) Space-filling representations of the ligand- and channel-binding surfaces of ShK and Kv1.3 (top) and ShK-Dap22 and Kv1.3 (bottom). Colored residues indicate those involved in the binding surfaces (based on changes in solvent-accessible surface area upon binding). The channel model in both cases is viewed from above, and each ligand molecule is rotated 180° perpendicular to the plane of the page in order to visualize their binding surfaces.

contrasts with their observed high-affinity binding and emphasizes that the models have scope for further refinement.

Figure 3C shows that the Kv1.3-binding surface of ShK incorporates most of the residues reported by Pennington et al. (*14*) and Rauer et al. (*15*) to be part of the essential binding surface. Arg11, Ser20, Lys22, Tyr23, and Phe27 were identified in both studies as important for K^+-channel binding. Rauer et al. (*15*) found Ile7 to be less important for

binding to Kv1.3 but also identified contributions from Thr13, His19, Met21, Arg24, Leu25, and Arg29. It is likely that Thr13 and His19 have a role in stabilizing the toxin structure (*28*, *29*), and therefore may not interact directly with the channel. Residues 11, 21, 22, 23, 25, 27, and 29 all experience some change in solvent accessibility as a result of binding to Kv1.3 (Figure 3B), but neither Ile7 nor Ser20 experiences any appreciable change. This is in spite of the fact that Ser20 is in close proximity (within 5 Å) to Gly401, Asp402, and His404 (from the subunit adjacent to the Arg11−His404 interaction). Similarly, Ile7 is within 5 Å of Val406 (from the subunit adjacent to the Arg11−His404 interaction), suggesting the potential for a hydrophobic interaction between the two.

Tyr23 is a conserved residue across the family of K^+-channel blocking toxins from sea anemones and is part of the conserved diad found in sea anemone and scorpion channel blockers. In the ShK−Kv1.3 model, Tyr23 sits within 5 Å of Gly401, Asp402, and His404 from the same subunit to which Arg11 is coupled. Similarly, the other aromatic residue in the essential binding surface of ShK, Phe27, is within 5 Å of Gly401, Asp402, Met403, Ser378, Ser379, His404, and Val406. Mutant cycles have been performed for only Phe27−His404, but the low $\Delta\Delta G$ value (0.06 kcal·mol^{-1}) suggests that these two residues do not interact. It is important to recall that, although high $\Delta\Delta G$ values indicate tight interactions (*21*), residues that are physically close may be energetically "silent" and not be detected using mutant cycle analysis (*18*, *21*). Indeed, Schreiber and Fersht (*21*) observed that interactions involving at least one uncharged side chain were less likely to show strong couplings in mutant cycle experiments, so the results for Phe27 are not unexpected. In the barnase−barstar complex, interactions of Trp38 with Lys27 and Arg59 gave relatively weak interaction energies even though these side chains were <4 Å apart in the crystal structure of the complex (*21*).

The interaction observed between Arg29 and Asp386 (Figure 1) contrasts with the finding by Rauer et al. (*15*) that Arg29 makes a relatively minor contribution to the binding of ShK to Kv1.3. Recent data on ShK−Kv1.3 binding (*15*) implicate Arg24 as important for channel binding. In our model, the side chain of Arg24 is oriented slightly away from the channel, approximately 9 Å from the closest channel residue, Ser379. Mutant cycle data not used in the docking simulations indicate that these two side chains are weakly coupled ($\Delta\Delta G = 0.5-0.8$ kcal·mol^{-1}), suggesting that these side chains are closer than in the model but supporting the overall docking configuration.

Why Does ShK-Dap22 Bind to Kv1.3 Differently from ShK? It was initially expected that ShK-Dap22 would bind to Kv1.3 in the same way as ShK. The shorter Dap side chain was expected to interact more strongly with Asp402 than with Tyr400, located deeper in the ion selectivity filter, as in fact observed (Figure 1), but Dap22 is also strongly coupled to channel residues further out in the vestibule, namely, Asp386 and His404. The distance between diagonally opposite Asp386 side chains is approximately 32 Å ($C^\gamma-C^\gamma$ distance), suggesting that, with Dap22 located at the mouth of the pore, the distance to any one Asp386 residue would be at least 16 Å. Thus, the strong coupling observed between Dap22 and Asp386 forces this analogue to bind to Kv1.3 in a different fashion from ShK. Both Arg11 and Arg29 make similar contacts with the channel to those in ShK, namely, to Asp386/His404 and Asp386, respectively. By contrast, both Ser20 and Phe27 of ShK-Dap22 are energetically coupled to either Asp386 and/or His404, whereas no such interactions were observed for the equivalent residues of ShK.

The dramatic difference in binding orientations for ShK and ShK-Dap22 was unexpected given that only a single residue mutation distinguishes the two. The solution structures of the two ligands are quite similar (*10*, *11*). Local differences in the relative orientations of some side chains have been noted; in particular, the key side chains of Dap22, Tyr23 and Arg11, appear to be more tightly clustered in ShK-Dap22 than in ShK. The effect of such minor differences would be difficult to detect at the resolution of our models, and so local structural differences are unlikely to be responsible for the different patterns of binding between ShK and ShK-Dap22. The possibility that one or both ligands undergoes significant structural change upon channel binding cannot be excluded, but seems unlikely given that the mutant cycle data for both can be satisfied quite well based on the structures of the free ligands.

The pore of Kv1.3 remains unoccupied when ShK-Dap22 is bound. Moreover, there is no ShK-Dap22 side chain in the vicinity of the pore that might be able to occupy the channel opening. The shorter side chain of Dap22, while not able to orient itself deep into the channel pore and directly effect blockade, is free to make other channel contacts, which appear to be sufficient for potent binding. Is this binding configuration unique for ShK-Dap22 and Kv1.3? Substitution of Lys27 in scorpion toxins with shorter residues such as Dap, Orn, and Ala has been used previously to establish the role of this residue in pore blockade (*16*, *17*). The trend observed is for the shorter side chain to make less of an interaction with Tyr400 and more with Asp402 and His404. However, the interactions of Dap residues with Asp386 have not been studied in these cases, so there is insufficient evidence from the literature to rule out the possibility that Dap-substituted analogues of scorpion toxins might bind to Kv1.3 in a fashion similar to that of ShK-Dap22. In fact, a Dap27 analogue of kaliotoxin was only ~3-fold less potent against Kv1.3 than the native toxin, perhaps indicating new toxin−channel interactions following the Lys to Dap substitution. Our findings emphasize the importance of obtaining numerous restraints from mutant cycle experiments undertaken with several different toxin and channel mutants in attempting to define docking configurations.

Why Is ShK-Dap22 More Selective than ShK for Kv1.3? ShK and ShK-Dap22 bind Kv1.3 with very similar potencies (*10*), so there is no significant energetic penalty associated with the different binding configurations. However, while ShK is similarly potent against Kv1.1 and only ~15-fold less potent against Kv1.6, ShK-Dap22 is ~80- and ~450-fold less potent against these same channels, respectively (*10*). One possible explanation for the selectivity achieved by ShK-Dap22 is subtle differences in pore topology between these channels, mediated by specific residue substitutions. Comparing the amino acid sequences for Kv1.1, -1.3, and -1.6, the most obvious difference lies in the vestibule region, in particular at position 404 (using Kv1.3 numbering). In Kv1.3, this position is occupied by His, and it has been

shown that a number of residues from ShK, ShK-Dap22, and various scorpion toxins interact with it (see above). In Kv1.1 and -1.6, this residue is a Tyr. It is unlikely that the selectivity is driven solely by the Dap22−His404 interaction since mutating His404 to Tyr (thereby making the channel more like Kv1.1 in this region) does not alter the affinity of ShK-Dap22 for Kv1.3 (K_d = 4.3 ± 2.5 pM). Kv1.3 and Kv1.1 differ in the P-region by only eight residues, but four are nonconservative mutations: Pro377 (Ala in Kv1.1), Thr378 (Glu), Gly380 (His), and Ser382 (Asn). Of these four mutations, Gly380 is the only one close to the ShK-Dap22 binding region of Kv1.3. Because of the interaction of ShK-Dap22 Arg11 with Ser379, the distance from Arg11 to Gly380 is approximately 4 Å. In Kv1.1, this position is occupied by histidine, and perhaps the difference in steric bulk at this position would be sufficient to alter the orientation of Arg11. However, the model of ShK bound to Kv1.3 has Arg11 a similar distance from Gly380, suggesting that differences in Kv1.1 and Kv1.3 at this position are unlikely to mediate the selectivity of ShK-Dap22. Likewise, Arg29 of both toxin molecules is located a similar distance from Gly380 in both models.

It appears that, with the Dap22 side chain being too short to occupy the pore, the toxin is no longer constrained to bind in the same way as the native toxin. Indeed, the new interactions made by ShK-Dap22 with the vestibule region of Kv1.3 may account for that fact that it binds tightly to this channel but not to others, and may be a key factor in its specificity for Kv1.3. Perhaps in other K^+-channels the Dap22 side chain makes the predicted interactions with the mouth of the pore and adopts a similar docked configuration to ShK in those channels, but with a lower affinity, reflecting the less favorable interactions of Dap22 compared with Lys22 in the pore. The fact that the selectivity of ShK-Dap22 for Kv1.3 is not attributable only to interactions of the Dap22 side chain with the ring of His404 residues in Kv1.3 supports the view that this analogue docks differently from ShK, driven by different side chain interactions from those for ShK. In this context, it is noteworthy that a scorpion toxin which is selective for the HERG K^+-channel has been shown very recently to interact with the outer vestibule of HERG and may not physically occlude the pore (*30*), as we are proposing for the interaction of ShK-Dap22 with Kv1.3.

Evaluation of the Kv1.3 Model and Docking Procedure. Whereas Kv1.3 is a six-transmembrane, voltage-gated potassium channel, KcsA (*31*), on which our Kv1.3 model was based, is a pH-gated potassium channel containing only two transmembrane regions per subunit. Yellen and co-workers (*32*) have suggested that the intracellular portion of voltage-gated K^+-channels may not be identical with the KcsA structure. Furthermore, the X-ray crystal structure of KcsA and the theoretical model of Shaker provide conflicting explanations as to the mechanism by which the selectivity of these channels for K^+ is mediated. Nevertheless, considerable evidence supports the view that potassium channels possess a conserved topology in their pore−vestibule regions. In particular, KcsA can be rendered sensitive to blockade by agitoxin 2 via the substitution of only three vestibule residues, two of which correspond to residues found in the sequence of Shaker (*33*). Therefore, it is reasonable to assume that the P-region of KcsA is an adequate analogue of the equivalent region of Kv1.3.

The models of ShK−Kv1.3 and ShK-Dap22-Kv1.3 represent approximations of how polypeptide toxins bind to a voltage-gated potassium channel. Determining the precise orientation of toxin with channel is limited by the fact that water was not taken into consideration in these binding simulations (*34*) in the interest of optimizing computation times. Water plays an important role in protein−protein interfaces, which contain at least as many water-mediated interactions as hydrogen bonds or salt bridges. The 'O-ring' model, proposed by Bogan and Thorn (*35*), places critical residues at the center of a ring and less critical residues at the periphery, with the free energy of water-mediated interactions on the periphery essentially equivalent to that of a direct hydrogen bond. On the other hand, water molecules included in the docking simulations also have the potential to adopt positions that cannot be checked by mutant cycle analyses and may be incorrect.

It is also important to note that our docking simulations are based on conservative interpretation of pairwise interactions inferred from mutant cycle data. We have not attempted to impose shorter interresidue constraints where strong couplings were observed, even though Schreiber and Fersht (*21*) found that strong couplings did in fact correlate with distances <5 Å. As with NMR-based structure determination, a larger number of conservatively interpreted restraints is likely to be more reliable than a small number of precisely determined ones, and further restraints derived from mutant cycle analyses would permit further refinement of the toxin−channel structures. Nevertheless, we believe that the current data (22 pairwise interactions tested in the case of ShK and 16 in the case of ShK-Dap22, as summarized in Figure 1) provide a sufficient basis for concluding that the docking configurations of ShK and ShK-Dap22 differ from one another in the case of Kv1.3.

Conclusions. Using a combination of molecular modeling and experimentally derived distance constraints, the docking of both ShK and ShK-Dap22 with Kv1.3 has been investigated. ShK blocks the channel via interactions similar to those proposed for scorpion K^+-channel blockers whereas ShK-Dap22 appears to make different interactions. Our models help explain how ShK-Dap22 retains its potency for Kv1.3 and achieves selectivity for Kv1.3 over other voltage-gated potassium channels. ShK-Dap22 is apparently able to function as a potent and Kv1.3-selective blocker without recourse to occupation of the channel pore via a lysine side chain. This finding suggests that an effective channel blocking compound might be designed that, unlike ShK, interacts only with residues in the channel's vestibule. In relation to the use of mutant cycle data generally to guide docking studies, our findings emphasize the importance of numerous restraints derived from multiple experiments in producing a consistent model.

ACKNOWLEDGMENT

We thank Heike Wulff for helpful discussions during the course of this work and for her comments on the manuscript.

REFERENCES

1. Cahalan, M. D., and Chandy, K. G. (1997) *Curr. Opin. Biotechnol. 8,* 749−756.
2. Kath, J. C., Hanson, D. C., and Chandy, K. G. (1997) *Annu. Rep. Med. Chem. 32,* 181−190.

3. Lin, C. S., Boltz, R. C., Blake, J. T., Nguyen, M., Talento, A., Fischer, P. A., Springer, M. S., Sigal, N. H., Slaughter, R. S., Garcia, M. L., Kaczorowski, G. J., and Koo, G. C. (1993) *J. Exp. Med. 177*, 637−645.
4. Koo, G. C., Blake, J. T., Talento, A., Nguyen, M., Lin, S., Sirotina, A., Shah, K., Mulvany, K., Hora, D., Cunningham, P., Wunderler, D. L., McManus, O. B., Slaughter, R., Bugianesi, R., Felix, J., Garcia, M., Williamson, J., Kaczorowski, G., Sigal, N. H., Springer, M. S., and Feeney, W. (1997) *J. Immunol. 158*, 5120−5128.
5. Lewis, R. S., and Cahalan, M. D. (1995) *Annu. Rev. Immunol. 13*, 623−653.
6. Beeton, C., Wulff, H., Barbaria, J., Clot-Faybesse, O., Pennington, M. W., Bernard, D., Cahalan, M. D., Chandy, K. G., and Béraud, E. (2001) *Proc. Natl. Acad. Sci. U.S.A. 98*, 13942−13947.
7. Chandy, K. G., Cahalan, M., Pennington, M., Norton, R. S., Wulff, H., and Gutman, G. A. (2001) *Toxicon 39*, 1269−1276.
8. Gasparini, S., Danse, J.-M., Lecoq, A., Pinkasfeld, S., Zinn-Justin, S., Young, L. C., de Medeiros, C. C. L., Rowan, E. G., Harvey, A. L., and Ménez, A. (1998) *J. Biol. Chem. 273*, 25393−25403.
9. Castañeda, O., Sotolongo, V., Amor, A. M., Stöcklin, R., Anderson, A. J., Harvey, A. L., Engström, Å., Wernstedt, C., and Karlsson, E. (1995) *Toxicon 33*, 603−613.
10. Kalman, K., Pennington, M. W., Lanigan, M. D., Nguyen, A., Rauer, H., Mahnir, V., Paschetto, K., Kem, W. R., Grissmer, S., Gutman, G. A., Christian, E. P., Cahalan, M. D., Norton, R. S., and Chandy, K. G. (1998) *J. Biol. Chem. 49*, 32697−32707.
11. Tudor, J. E., Pallaghy, P. K., Pennington, M. W., and Norton, R. S. (1996) *Nat. Struct. Biol. 3*, 317−320.
12. Dauplais, M., Leqoc, A., Song, J., Cotton, J., Jamin, N., Gilquin, B., Roumestand, C., Vita, C., de Medeiros, C. L. C., Rowan, E. G., Harvey, A. L., and Ménez, A. (1997) *J. Biol. Chem. 272*, 4302−4309.
13. Pennington, M. W., Mahnir, V. M., Krafte, D. S., Zaydenberg, I., Byrnes, M. E., Khaytin, I., Crowley, K., and Kem, W. R. (1996) *Biochem. Biophys. Res. Commun. 219*, 696−701.
14. Pennington, M. W., Mahnir, V. M., Krafte, D. S., Khaytin, I., Zaydenberg, I., Byrnes, M. E., and Kem, W. R. (1996) *Biochemistry 35*, 16407−16411.
15. Rauer, H., Pennington, M. W., Cahalan, M. D., and Chandy, K. G. (1999) *J. Biol. Chem. 274*, 21885−21892.
16. Alessandri-Haber, N., Lecoq, A., Gasparini, S., Grangier-Macmath, G., Jacquet, G., Harvey, A. L., de Medeiros, C., Rowan, E. G., Gola, M., Ménez, A., and Crest, M. (1999) *J. Biol. Chem. 274*, 35653−35661.
17. Aiyar, J., Withka, J. M., Rizzi, J. P., Singleton, D. H., Andrews, G. C., Lin, W., Boyd, J., Hanson, D. C., Simon, M., Dethlefs, B., Lee, C.-L., Hall, J. E., Gutman, G. A., and Chandy, K. G. (1995) *Neuron 15*, 1169−1181.
18. Ranganathan, R., Lewis, J. H., and MacKinnon, R. (1996) *Neuron 16*, 131−139.
19. Aiyar, J., Rizzi, J. P., Gutman, G. A., and Chandy, K. G. (1996) *J. Biol. Chem. 271*, 31013−31016.
20. Yao, X., Liu, W., Tian, S., Rafi, H., Segal, A. S., and Desir, G. V. (2000) *J. Biol. Chem. 275*, 10859−10863.
21. Schreiber, G., and Fersht, A. R. (1995) *J. Mol. Biol. 248*, 478−486.
22. Rauer, H., Lanigan, M. D., Pennington, M. W., Aiyar, J., Ghanshani, S., Cahalan, M. D., Norton, R. S., and Chandy, K. G. (2000) *J. Biol. Chem. 275*, 1201−1208.
23. Koradi, R., Billeter, M., and Wüthrich, K. (1996) *J. Mol. Graphics 14*, 51−55.
24. Lawrence, M. C., and Colman, P. M. (1993) *J. Mol. Biol. 234*, 946−950.
25. Stanfield, R. L., and Wilson, I. A. (1995) *Curr. Opin. Struct. Biol. 5*, 103−113.
26. Janin, J. (1999) *Structure 7*, R277−R279.
27. Epa, V. C., and Colman, P. M. (2001) *Curr. Top. Microbiol. Immunol. 260*, 45−53.
28. Tudor, J. E., Pennington, M. W., and Norton, R. S. (1998) *Eur. J. Biochem. 251*, 133−141.
29. Lanigan, M. D., Tudor, J. E., Pennington, M. W., and Norton, R. S. (2001) *Biopolymers 58*, 422−436.
30. Pardo-Lopez, L., Zhang, M., Liu, J., Jiang, M., Possani, L. D., and Tseng, G. N. (2002) *J. Biol. Chem. 277*, 16403−16411.
31. Doyle, D. A., Cabral, J. M., Pfuetzner, R. A., Kuo, A., Gulbis, J. M., Cohen, S. L., Chait, B. T., and MacKinnon, R. (1998) *Science 280*, 69−77.
32. del Camino, D., Holmgren, M., Liu, Y., and Yellen, G. (2000) *Nature 20*, 321−325.
33. MacKinnon, R., Cohen, S. L., Kuo, A., Lee, A., and Chait, B. T. (1998) *Science 280*, 106−109.
34. Sansom, M. S. P., Shrivastava, I. H., Ranatunga, K. M., and Smith, G. R. (2000) *Trends Biochem. Sci. 25*, 368−374.
35. Bogan, A. A., and Thorn, K. S. (1998) *J. Mol. Biol. 280*, 1−9.

BI026400B